Cellular and Molecular Life Sciences (2025) 82:95
https://doi.org/10.1007/s00018-024-05542-3

ORIGINAL ARTICLE

AXL promotes lymphangiogenesis by amplifying VEGF-C-mediated AKT pathway

Sébastien Pirson[1] · Marine Gautier-Isola[1] · Louis Baudin[1] · Loïc Rouaud[1] · Aline Vanwynsberghe[1] · Jonathan Deroye[1] · Sophie Bekisz[1,2] · Fabrice Gucciardo[1] · Alizée Lebeau[1] · Florence Buntinx[1] · Elitsa Ivanova[1] · Bernard Staumont[2] · Silvia Blacher[1] · Christine Gilles[1] · Agnès Noël[1,3,4]

Received: 27 May 2024 / Revised: 23 September 2024 / Accepted: 6 December 2024

Abstract

Lymphangiogenesis has gained considerable interest due to its established role in cancer progression and dissemination of metastatic cells through lymph nodes. Deciphering the molecular mechanisms that govern lymphangiogenesis within lymph nodes holds promise for revealing novel targetable molecules and pathways to inhibit metastasis. In this study, we revealed a previously unrecognized role of AXL, a tyrosine kinase receptor, in the lymphatic vessel formation. We first validated the expression of AXL in lymphatic endothelial cells (LECs), followed by functional studies using RNA interference and pharmacological inhibition with R428/Bemcentinib. These approaches provided compelling evidence that AXL promotes LEC migration in both 2D and 3D culture systems. Our findings demonstrated that AXL activation was induced by VEGF-C (Vascular Endothelial Growth Factor C) and further amplified downstream signaling via the AKT pathway. In vivo, the role of AXL in lymphatic vessel sprouting was demonstrated using R428 in a model of VEGF-C-induced lymphangiogenesis in lymph nodes. Interestingly, we discovered that AXL was predominantly expressed in $MARCO^{+}$ LECs. Strikingly, under metastatic conditions, there was a notable increase in the density and penetration extent of these AXL-expressing LECs into the lymph node parenchyma. Collectively, our findings pinpoint AXL as a potent enhancer of lymphangiogenesis operating through the VEGF-C/AKT pathway. Furthermore, the identification of AXL expression within a distinct LEC subpopulation, particularly in the context of metastasis, underscores the intricate interplay between AXL signaling and lymphatic dynamics within the lymph node microenvironment.

Keywords Lymphangiogenesis · AXL · VEGF-C pathway · Lymph node · R428/Bemcentinib · AKT pathway

Introduction

The evaluation of lymph node (LN) status is critical to determine the stage of cancer progression. The detection of tumor cells in the sentinel LN is a crucial prognostic indicator guiding treatment decisions for patients with breast, cervical, prostate cancers or melanomas [1–4]. However, prior to nodal dissemination, important tissue alterations are induced by the primary tumor. Some tumor cells have the capacity to precondition the sentinel LN by secreting soluble factors or extracellular vesicles. These factors trigger substantial matrix remodelling, immune system modulation, angiogenesis and lymphangiogenesis [5–7]. This pre-conditioning of LN facilitates the survival and proliferation of disseminating tumor cells. Metastases in the LN can potentially spread to distant organs, contributing to

Sébastien Pirson, Marine Gautier-Isola, Christine Gilles and Agnès Noël contributed equally to this work.

✉ Agnès Noël
agnes.noel@uliege.be

1 Laboratory of Tumor and Development Biology, GIGA-Cancer, Liege University, Liege, Belgium

2 Biomechanics Research Unit, GIGA In Silico Medicine, ULiège, Liège, Belgium

3 Walloon Excellence in Life Sciences and Biotechnology (WELBIO), Wavre, Belgium

4 Laboratory of Tumor and Development Biology, GIGA-Cancer, Tour de Pathologie, B23, +4, Avenue Hippocrate, 13, Liège 4000, Belgium

Published online: 27 February 2025

secondary metastases that often evade current treatment modalities [8–12].

Recent advances in single-cell RNA sequencing (scRNA-seq) have unveiled a remarkable heterogeneity of lymphatic endothelial cells (LECs) within the LN. Multiple distinct LEC subsets have been identified in both human and murine LNs [13–16]. Numerous factors contribute to lymphangiogenesis and include for instances Hepatocyte Growth Factor (HGF) and Vascular Endothelial Growth Factors (VEGFs) [6]. VEGF-C is the main lymphangiogenic factor, which primarily binds to VEGFR-3 (Vascular Endothelial Growth Factor Receptor-3), forming homodimers or heterodimers with VEGFR-2. Moreover, VEGFR-2 and VEGFR-3 interact with various cell surface molecules acting as co-receptors (neuropilins and heparan sulfate proteoglycans) or non-VEGF-binding auxiliary proteins (e.g. integrins, ephrin B2, VE-cadherin and uPARAP/Endo180) [17–20]. VEGF-C primarily activates RAS/MAPK (Mitogen-Activated Protein Kinase) and PI3K/AKT (Phosphoinositide 3-Kinase/Protein Kinase B) pathways promoting LEC survival, migration, and proliferation. Notably, PI3K/AKT has emerged as a key regulator of lymphatic vascular development [21]. The p85 regulator subunit of PI3K can directly interact with VEGFR-3, but not with VEGFR-2 [22]. Nevertheless, VEGFR-2 can activate the PI3K/AKT pathway in an indirect manner in blood endothelial cells [23].

AXL, a receptor tyrosine kinase (RTK) within the TAM family (TYRO3, AXL and MERTK) is expressed in diverse cell types, including macrophages, fibroblasts, endothelial cells and cancer cells [24]. AXL is involved in several processes associated to cancer progression including cancer cell survival, proliferation, migration, invasion, drug resistance, Epithelial-Mesenchymal Transition (EMT), immune evasion and angiogenesis [24]. Growth arrest-specific 6 (GAS6), classified as a vitamin K-dependent protein, demonstrates a high affinity for binding AXL and is considered as the main ligand of AXL [25]. Nevertheless, AXL activation is not exclusively dependent on its interaction with GAS6. It can be triggered by alternative mechanisms such as heterodimerization or cross-talk with other RTKs, including Epithelial Growth Factor Receptor (EGFR) and Human Epidermal Growth Factor Receptor-2 (HER2) [26]. Additionally, indirect AXL activation has been reported in blood endothelial cells following the activation of VEGF-A pathway and SRC signaling [23]. Despite the well-known roles of AXL in cancer progression and in angiogenesis, AXL involvement in tumoral lymphangiogenesis, as well as the subsequent signalling network it triggered in LECs, warrant further exploration.

Given the absence of reported implication of AXL in lymphatic biology, we sought to investigate its role in lymphangiogenesis associated with LN metastases. Through a combination of in vitro models and in vivo ear sponge assays mimicking LN metastases [27], we here assign a novel function of AXL in the lymphangiogenic process. We further implicate AXL in the VEGF-C/VEGFR-2/-3/AKT pathway, offering the possibility to target this axis with anti-AXL drugs.

Results

AXL is expressed by LECs and promotes their migration

Our initial analyses by RT-qPCR and Western Blotting revealed the expression of AXL in human dermal LECs (HMVEC-dLy) (Fig. 1A, B). To further evaluate a potential functional role of AXL in lymphangiogenesis, we next downregulated AXL expression through siRNA silencing. Cell transfection with a pool of 3 siRNAs against AXL (siAXL) led to a drastic reduction of AXL both at the mRNA and protein levels (Fig. 1A, B). AXL silencing led to a significant reduction of LEC migration, as evaluated in a scratch wound healing assay performed with or without VEGF-C (Fig. 1C, D). Specifically, in untreated cells, the recovery of the wounded area reached 27% in siCTRL cells *versus* 17% in siAXL cells. In VEGF-C treated cultures, the area recovery was 39% in siCTRL cells *versus* 21% in siAXL cells ($p < 0.05$) (Fig. 1C, D). Notably, the involvement of AXL in cell migration was supported by an inhibition of LEC migration in the presence of mitomycin C, an antiproliferative drug ($p < 0.05$) (Suppl. Figure 1A, B).

To enhance the stimulation of LEC sprouting, we employed a three-dimensional assay involving LEC spheroids embedded in a collagen gel (Fig. 1E, F, G). VEGF-C exhibited a remarkable capacity to induce sprouting, which was attenuated by AXL silencing (Fig. 1E, F). AXL silencing indeed significantly reduced the number of sprouts following VEGF-C stimulation (Fig. 1F) and affected the length of sprouting (Fig. 1G). Consistent with the findings from 2D wound healing assays, the inhibition of VEGF-C-induced LEC sprouting remained similar whether mitomycin C was present or absent, further validating the impact of AXL on cell migration (Suppl. Figure 1 C, D, E).

In addition to VEGF-C, we also examined other growth factors: GAS6, HGF, VEGF-A, and a mutated form of VEGF-C (VEGF-$C_{cys156ser}$) which exclusively binds to the VEGFR-3 receptor (Suppl. Figure 2A, B). AXL silencing reduced the number of sprouts across all other growth factor conditions. However, this decrease reached statistical significance only in spheroids treated with HGF and VEGF-$C_{cys156ser}$ (Suppl Fig. 2B). Next, the AXL inhibitor R428 was used to corroborate our findings in both 2D (wound healing)

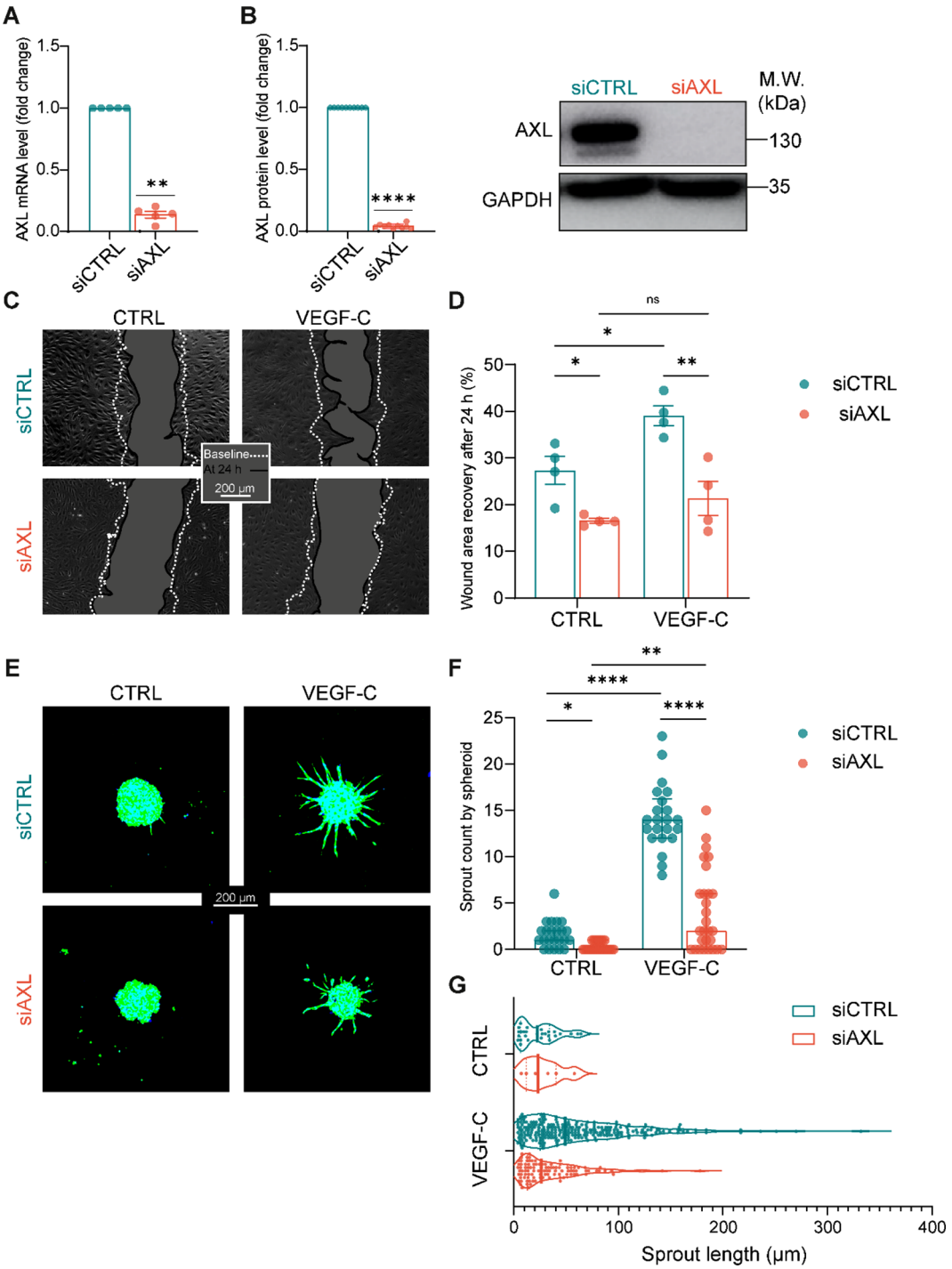

Fig. 1 Silencing AXL decreases LEC migration induced by VEGF-C. **A-B.** AXL expression monitored by RT-qPCR (**A**) and Western Blot (**B**) in LECs after transfection with a pool of 3 siRNAs against AXL (siAXL) or 3 control siRNAs (siCTRL). **C-D.** 2D-migration wound healing assay of transfected LECs stimulated without (control referred to CTRL) or with VEGF-C. Phase-contrast images (**C**) were acquired at 0 h and 24 h, enabling the quantification (**D**) of the area recovered by cells. **E-G.** 3D-spheroid sprouting assay performed with siRNA-transfected LECs stimulated or not (CTRL) with VEGF-C for 48 h. Confocal microscopy images of spheroids were acquired after 48 h of migration (CMFDA-stained cytoplasm and SPY-DNA-stained nuclei in green and in cyan, respectively (**E**). Sprout enumeration was performed (**F**) and the distribution of sprout length was analyzed (**G**). **A**, **B**, **D.** Data are means ± SEM from at least 3 independent experiments. **F**, **G**. Data are medians with interquartile ranges. Spheroid number ≥ 18 from 7 independent experiments. Statistical tests: One sample t test (**A**, **B**), two-way ANOVA with Holm-Sidak post hoc test for multiple comparisons (**D**) and Kruskal-Wallis test followed by Dunn's multiple comparisons test (**F**). ns: non-significant, *$p<0.05$, **$p<0.01$, ****$p<0.0001$

and 3D (spheroid) assays. Determining the appropriate dose of R428 was achieved through a caspase 3/7-based cytotoxic assay (Suppl. Figure 3 A). Consistent with the aforementioned data, a non-cytotoxic dose of R428 (0.75 µM) decreased LEC migration in wound healing (Fig. 2A, B) and spheroid assays (Fig. 2C, D, E), with or without mitomycin C (Suppl. Figure 3B-F) when LECs were stimulated with VEGF-C. Furthermore, among other growth factors examined, LECs stimulated by VEGF-$C_{cys156ser}$ or VEGF-A were also significantly affected by R428 in terms of sprout number (Suppl. Figure 4).

Although silencing or inhibiting AXL impair LEC migration induced by various factors, our data collectively indicate that AXL plays a pivotal role in promoting LEC migration and sprouting mediated by VEGF-C, recognized as the most potent lymphangiogenic factor. Furthermore, it can be effectively and consistently targeted by both siRNA and pharmacological approaches.

AXL is activated by VEGF-C and amplifies the downstream AKT signaling pathway

To precise a role for AXL in the response induced in LECs by VEGF-C, we first conducted a kinetic analysis of the phosphorylation of AXL and AKT, as a downstream effector of PI3K activity. Upon VEGF-C stimulation, a rapid phosphorylation of AXL was detected, peaking at 30 min (Fig. 3A). AKT phosphorylation reached its maximum level earlier, within the first 15 min of stimulation, and was still detected after 30 min. AXL inhibition by siRNAs or particularly with R428 decreased AKT phosphorylation following VEGF-C stimulation (Fig. 3B, C). Assessing pAKT kinetic in LECs treated with VEGF-A and VEGF-$C_{cys156ser}$ similarly revealed a reduction in pAKT in the presence of siAXL or R428 (Suppl. Figure 5).

These findings support a crosstalk between AXL and VEGFR-2/VEGFR-3. This prompted us to test whether AXL and VEGF receptors can form molecular complexes through co-immunoprecipitation approaches. Both VEGFR-2 and VEGFR-3 co-immunoprecipitated with AXL in basal conditions (Fig. 3D).

In vivo VEGF-C-driven lymphangiogenesis is inhibited by R428

To assess the functional relevance of AXL in LN-associated lymphangiogenesis in vivo, we implanted cell-free gelatin sponges in the ear of mice (between the external ear skin layer and the cartilage). VEGF-C (1 µg) was repeatedly administrated in the sponges to induce lymphangiogenesis in the sentinel LN (SLN, corresponding to the superficial parotid LN). This method enabled us to assess the effect of VEGF-C while circumventing the potential impact from tumor cell-derived AXL. Increasing doses of R428 (ranging from 1.9ng to 7.6ng) were repeatedly injected in mice ear every 3 days (Fig. 4A). At the end of the experiment, the SLN and the distant LN (DLN, corresponding to the mandibular LN), used as a control, were dissected. The density of LYVE-1^+ lymphatic vessels was quantified using a computer-assisted method. An increased LYVE-1 staining density in SLNs ($p<0.05$) was observed following local VEGF-C administration, compared to corresponding unstimulated controls (DMSO) (Fig. 4B, C). R428 injections resulted in a dose-dependent reduction of VEGF-C-induced lymphatic vessel sprouting specifically in SLNs (Fig. 4B, C), while DLNs showed no significant change (Fig. 4B, D). This was evidenced by a reduction of both the total labelling density of LYVE-1 and the spatial distribution of lymphatic vessels after injection of 7.6 ng R428 ($p<0.05$) (Fig. 4B, C, E, F).

AXL is expressed in MARCO+ LECs of murine LN

Given the recently discovered heterogeneity of LECs in LNs, we explored whether AXL could be produced by specific sub-populations of LECs. As AXL staining extended into the perifollicular medulla, we focused our attention on Macrophage Receptor with Collagenous structure (MARCO)-LECs, which have been identified in this LN area. Immunostainings for AXL, LYVE-1, MARCO in naive SLN revealed AXL signals in a majority of, though not all, LYVE-1^+ lymphatic vessels (Fig. 5A). Interestingly, AXL signal was detected in a subpopulation of $MARCO^+$ cells.

To further expand these observations as well as those obtained on the in vivo tumor cell-free model to a tumoral context, we utilized a tumor cell-containing ear-sponge assay. We thus implanted gelatin sponges containing melanoma B16-F10 tumor cells in ears of mice, sacrificed the mice at day 28 and collected SLN for further immunostaining analyses (Fig. 5B). This revealed a substantial remodeling of the SLN (referred here as "tumor-draining LN" or Td LN) (Fig. 5C-F). Sham LNs from mice implanted with a cell-free sponge were examined as control. We thus performed AXL/LYVE-1/MARCO stainings and an AXL immunodetection combined with a RNAscope analysis of *Prox1* mRNAs, a specific transcription factor for LECs. Supporting our observations made on naive LN above (Fig. 5A), AXL was detected in a majority, but not all, LYVE-1 and *Prox1* mRNA expressing cells (Fig. 5C and G). Importantly, while AXL expression in $MARCO^+$ LECs was observed in both sham and Td LNs (Fig. 5C), the densities of LYVE-1, AXL and MARCO stainings were found enhanced in Td LNs compared to sham LNs (Fig. 5D)

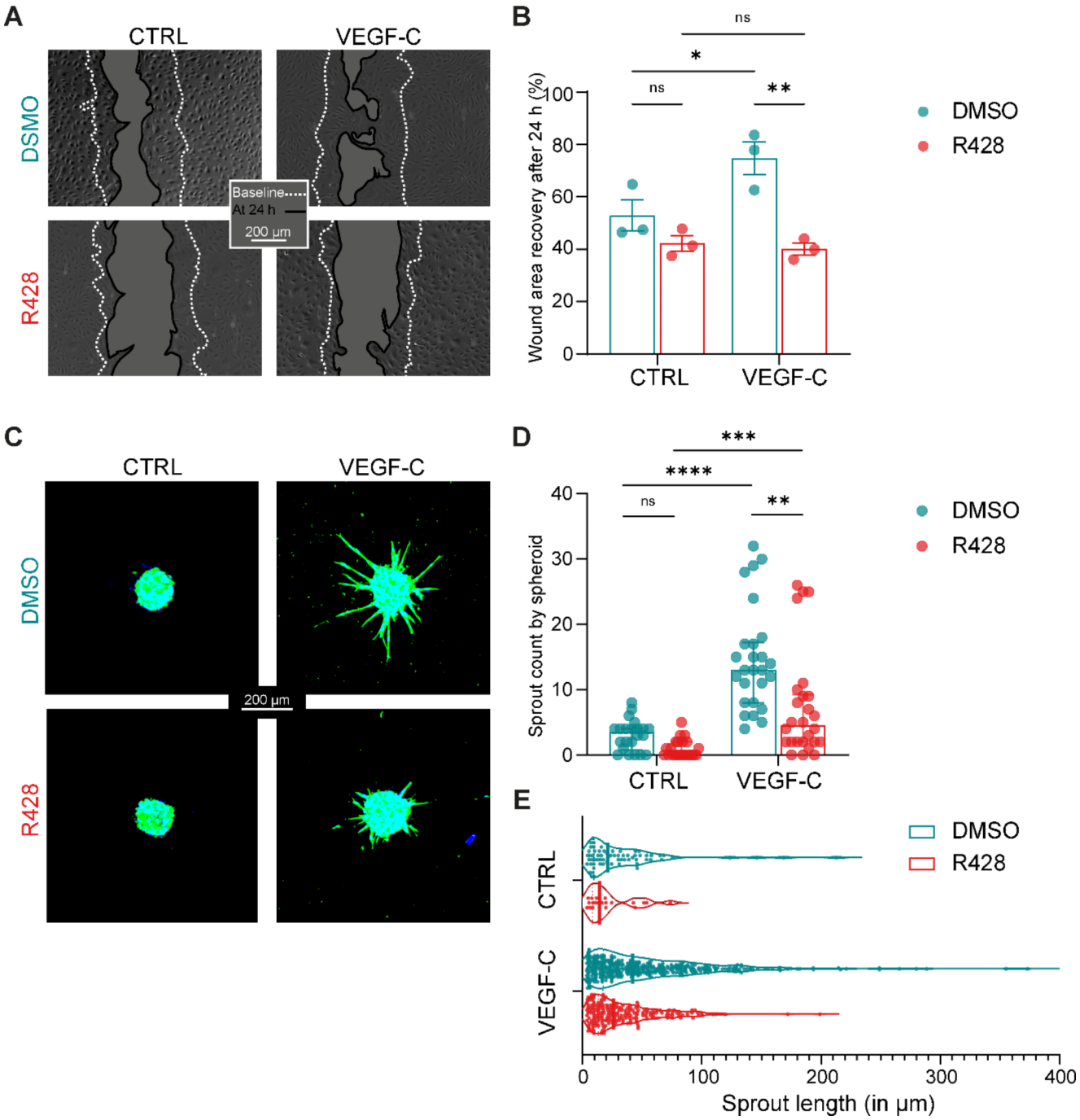

Fig. 2 R428 decreases LEC migration induced by VEGF-C. **A-B**. 2D-migration wound healing assay of LECs treated (R428) or not (DMSO) with R428 (0.75µM) and stimulated without (CTRL) or with VEGF-C. Phase-contrast images (**A**) were acquired at 0 h and 24 h, enabling the quantification (**B**) of the area recovered by cells. **C-E.** 3D-spheroid sprouting assay performed with LECs treated (R428) or not (DMSO) with R428 and stimulated or not (CTRL) with VEGF-C for 48 h. Confocal microscopy images of spheroids were acquired after 48 h of migration (CMFDA-stained cytoplasm and SPY-DNA-stained nuclei are in green and in cyan, respectively) (**C**). Sprout enumeration was performed (**D**) and the distribution of sprout length was analyzed (**E**). **B.** Data are means ± SEM from 3 independent experiments. **D**, **E.** Data are medians with interquartile ranges. Spheroid number ≥ 18 from **7** independent experiments. Statistical tests: two-way ANOVA with Holm-Sidak post hoc test for multiple) comparisons (**B**) and Kruskal-Wallis test followed by Dunn's multiple comparisons test (**D**). ns: non-significant, *$p<0.05$, **$p<0.01$, ****$p<0.0001$

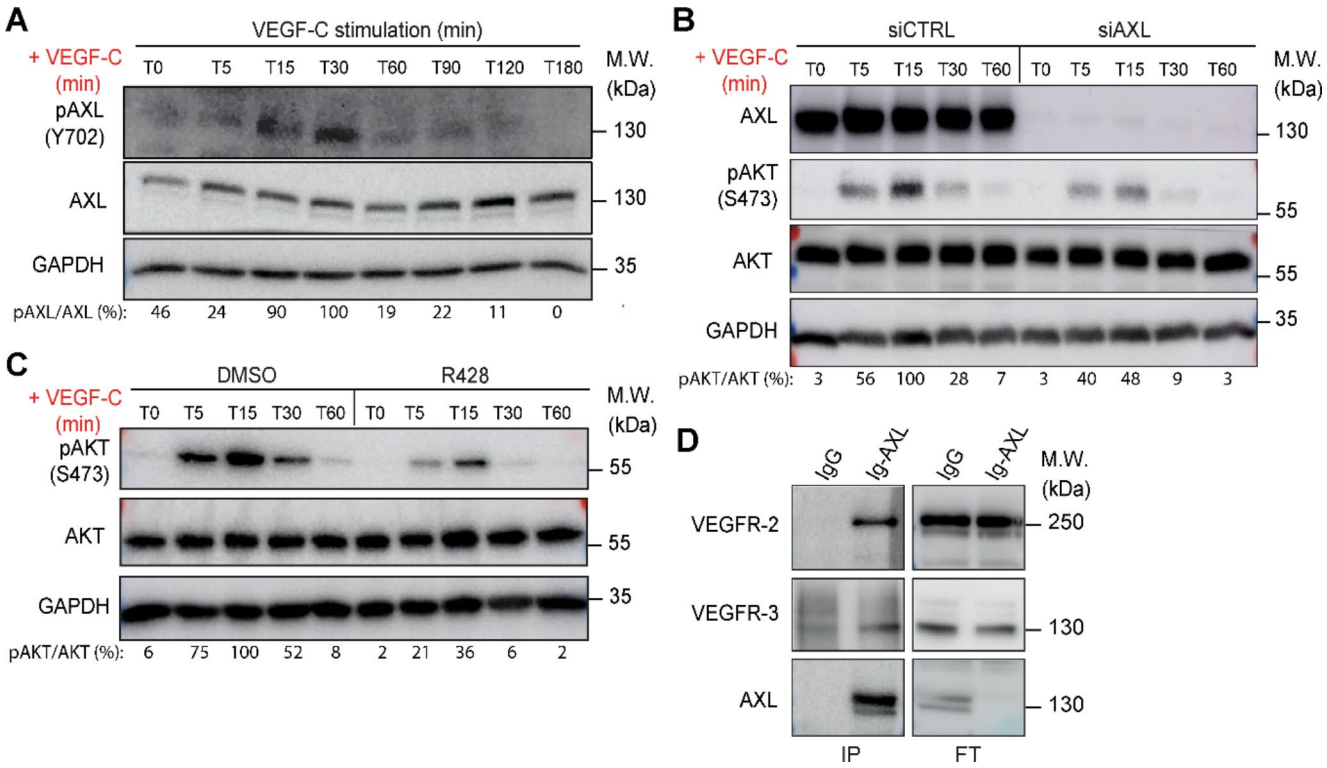

Fig. 3 AXL activation induced by VEGF-C amplifies AKT signaling pathway. **A-C.** Western blot analyses of pAXL, AXL, pAKT or AKT (as indicated) in LECs stimulated with VEGF-C for different time points (**A**), and silenced or not for AXL by siRNA (**B**), or treated or not (DMSO) with R428 (0.75 µM) (**C**). **D.** Co-immunoprecipitation analysis. Western blot of VEGFR-2, VEGFR-3 and AXL in AXL immunoprecipitates (IP) or in the flow through fractions (FT) were performed. For the kinetic analyses, an indicative quantification of band intensity was conducted and expressed as percentage of the highest pAKT/AKT ratio, normalized to 100%

($p<0.05$). These LYVE-1$^+$/AXL$^+$/MARCO$^+$ LECs also infiltrated deeper into the parenchyma of Td LNs than those in the sham group (Fig. 5E, F) ($p<0.05$), supporting their implication in tumor-induced lymphangiogenic remodeling.

Discussion

LECs play a major role in the metastatic dissemination process into LNs. It is now recognized that the lymphatic vasculature undergoes significant remodeling during the formation of a pre-metastatic niche before the arrival of cancer cells [1]. However, our understanding of the signaling dynamics between the main lymphangiogenic factor VEGF-C and its receptors, as well as co-receptors, remains incomplete. This study elucidates a novel pathway involving VEGF-C signaling through the receptor tyrosine kinase AXL and the AKT signaling cascade. These conclusions are based on, (1) functional assays conducted in vitro through RNA interference and pharmacological inhibition of AXL in human LECs, (2) the dissection of VEGF-C signal integration in presence or absence of AXL, (3) a pharmacological approach applied to an in vivo model of VEGF-C- induced lymphangiogenesis, and (4) the characterization of AXL expression specifically in MARCO$^+$ LECs in tumor draining murine LNs. These analyses reveal an intricate connection between VEGF-C/VEGFR-2/R-3 signaling, AXL and the downstream AKT pathway within LECs, providing new insights into the mechanisms underlying tumor-associated lymphatic vessel remodeling in LNs.

We first documented AXL expression in LECs in vitro. Very few studies have explored this RTK in LECs. In agreement with our observations, Maria Nassar et al. reported AXL expression in murine gingival LECs [28]. Conversely, a previous report suggested that PROX1 expression might suppress AXL expression [29]. These somewhat contrasting observations suggest a multifactorial regulatory mechanism governing AXL expression in LECs. Most importantly, we here show a functional implication of AXL in LECs during lymphangiogenesis associated to VEGF-C-induced remodeling in LNs. Through RNA interference and pharmacological inhibition with R428, we provide the first evidence for AXL involvement in lymphangiogenesis. In vitro experiments demonstrated that AXL silencing reduced LEC migration in both 2D and 3D models. Although AXL has been mostly studied in tumor cells, it has also been shown to regulate migration, invasion and proliferation of blood endothelial cells (BECs) [30–32], supporting our

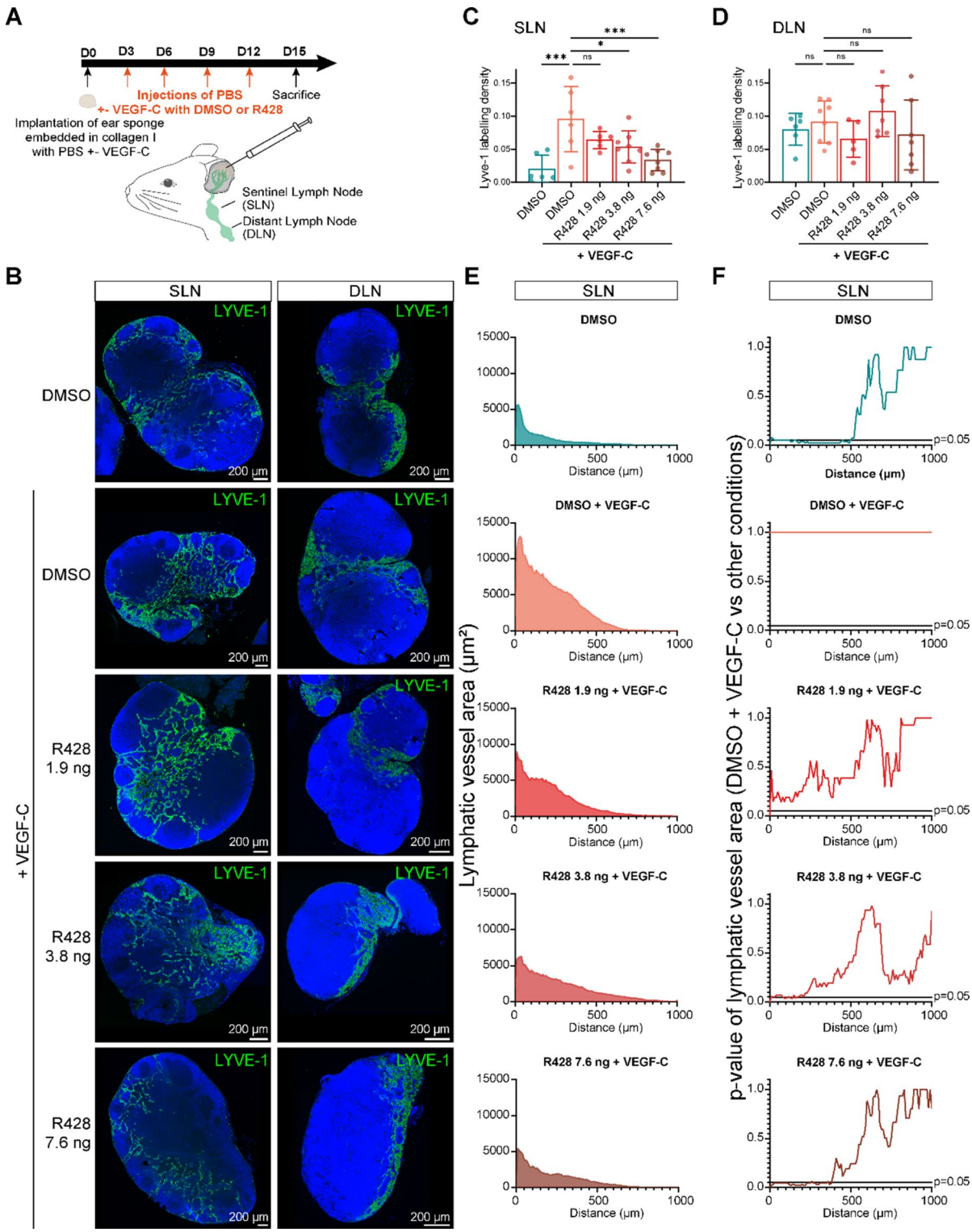

Fig. 4 R428 decreases VEGF-C-driven lymphangiogenesis in murine LN. **A-F.**In vivo lymphangiogenesis assays. The experimental design of the assay is depicted in (**A**). The assay was performed with or without VEGF-C, and with increasing doses of R428 (**B-F**). DMSO was used as a solvent control. Sentinel LNs (SLNs; Superficial parotid LNs) and distant LNs (DLNs; Mandibular LNs) were collected 15 days after sponge implantation. Images of LYVE-1 (lymphatic vessel immunostaining, green) and DAPI (nuclei, blue) staining were acquired (**B**). Computerized quantification of LYVE-1 staining density in SLN (**C**) and DLN (**D**), and analysis of spatial distribution in SLN (**E**, **F**) were performed. **B-D.** Data are means ± SEM. Statistical test: one-way ANOVA with Holm-Sidak post hoc test for multiple comparisons. *$p<0.05$, **$p<0.01$, ***$p<0.001$, ****$p<0.0001$. **E.** Data are vessel area medians according to the distance from the LN border (d = 0). **F**. Data are p-value of staining area differences with control (DMSO + VEGF-C) for each distance. Below the dotted line, p is lower than 0.05 and considered as significant. Statistical test: Mann–Whitney U test for each distance. $n \geq 6$ for each group

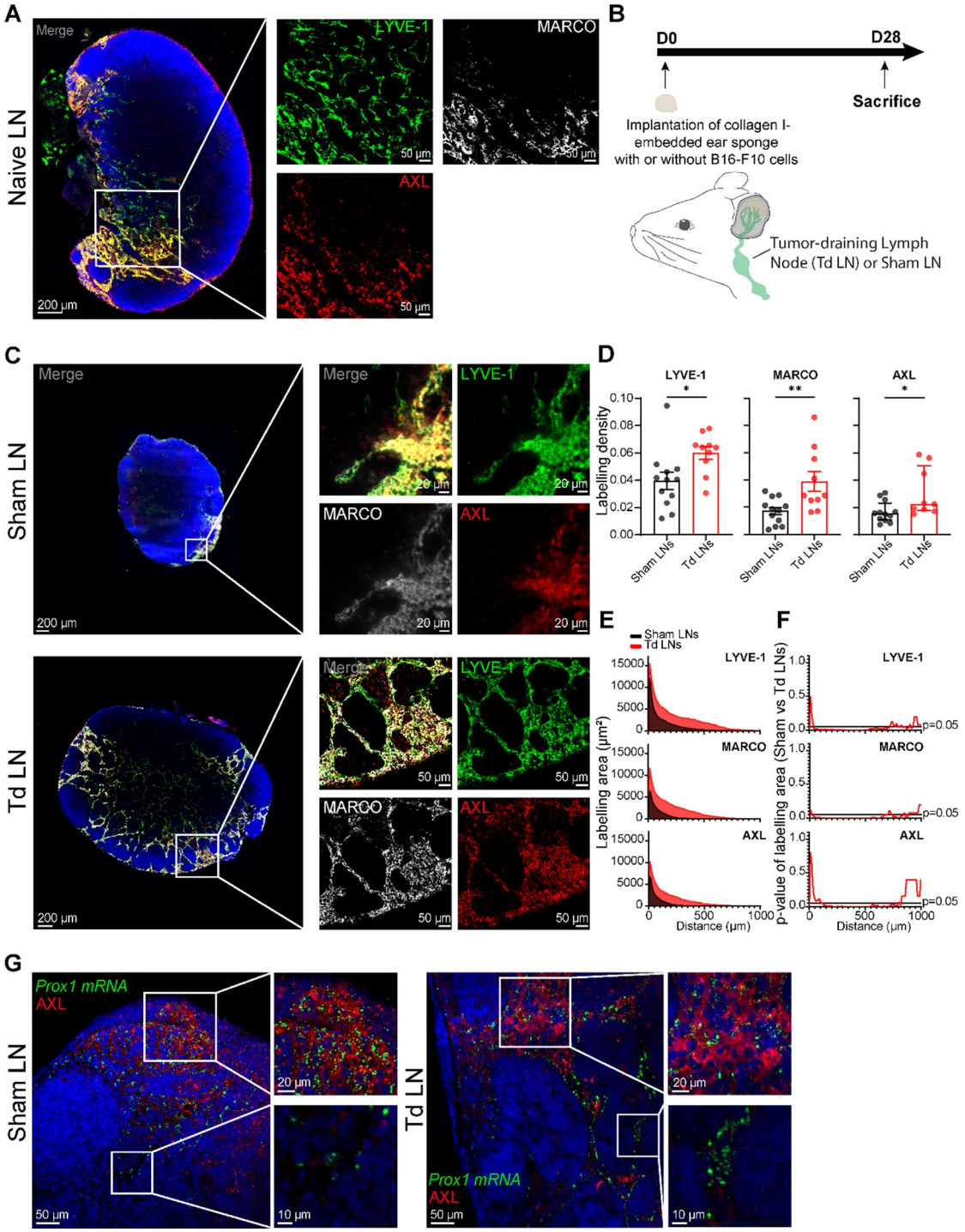

Fig. 5 AXL is expressed by MARCO^{+} LECs in murine LN. **A.** Representative images of naive murine lymph node immunostained for AXL (red), LYVE-1 (green), MARCO (white). **B-D**. In vivo Tumor-associated lymphangiogenesis assay. The experimental design of the assay is given in (**B**). Gelatin sponges containing (tumor draining: Td) or not (sham) melanoma cells were implanted in mice ear. The sentinel LN (Td LN or sham LN) were resected 28 days later. Images of AXL (red), MARCO (white), LYVE-1 (green) and DAPI (nuclei, blue) were acquired (**C**). Computerized quantification of the staining densities (**D**) and spatial distribution analysis (**E**, **F**) were performed in murine Sham and Td LNs. **D.** Data are means ± SEM for LYVE-1 and MARCO graphs and medians with interquartile ranges for AXL graph. Statistical tests: Unpaired t test (LYVE-1 and MARCO graphs) and Mann–Whitney U test (AXL graph). *$p<0.05$, **$p<0.01$. **E.** Data are staining area medians according to the distance from the LN border (d = 0). **F.** Data are p-values of staining area differences between Td and Sham LNs for each distance. Below the dotted line, p is lower than 0.05 and considered as significant. Statistical test: Mann–Whitney U test for each distance. $n \geq 7$ for each group. **G.** Images of *Prox1* RNA-scope hybridization (lymphatic vessel, green) and AXL immunostaining (red) in Sham and Td LNs

observation on LECs. Contrasting with its GAS6-dependent effects reported in BECs and cancer cells [32, 33], recombinant GAS6 failed to activate LECs possibly pointing to the implication of cell-type specific cofactor(s).

Mechanistically, we showed for the first time (i) the presence of AXL within molecular complexes involving VEGFR-3 and VEGFR-2 as assessed by co-immunoprecipitation assay, (ii) an inhibition of VEGF-C-induced AKT phosphorylation after AXL silencing or pharmacological inhibition. These results demonstrate the intricate relationship between AXL and the VEGF-C/VEGFR-2/-3 pathway, boosting the downstream AKT signaling pathway, which has been shown to be crucial for lymphangiogenesis [21, 22]. The involvement of both receptors in the process was further supported by our findings that silencing/inhibiting AXL also hinder VEGF-A and VEGF-Ccys156ser-induced LEC migration and sprouting. Functionally, the ear sponge assay [27, 34] was adapted and used to investigate LN lymphatic remodeling induced by VEGF-C *in vivo*. Its advantages include an accurate identification of sentinel and distant lymph nodes and high reproducibility of injections due to the well-defined injection site. Additionally, the constant volume is easily injectable into the space created by the sponge. This system allows to study the impact of LEC-expressed AXL on VEGF-C-induced lymphangiogenesis without interfering effects of tumor cell-derived AXL. Of great interest is our finding that R428 drastically reduced lymphatic sprouting in SLNs after VEGF-C stimulation. This provides a crucial additional insight into the role of R428 in LN remodeling. Indeed, numerous studies revealing significant reduction of metastasis by R428 rather highlight its impact on intrinsic pro-metastatic properties of tumor cells and, although less extensively, its impact on blood vessels [35–38]. We here demonstrate that the action of R428 is broader, also affecting lymphatic vessels which serve as a route for both LN and distant metastases [11].

Single-cell transcriptomic data have revealed several subtypes of LECs in LNs, suggesting functional heterogeneity in LECs [13–16]. In the present study, we established that AXL is expressed in a specific population of $MARCO^+$ LECs, mainly localized in the medullary/perifollicular zone of LN. The expression of AXL in $MARCO^+$ LECs and the enhancement of $MARCO^+/AXL^+$ LEC infiltration in tumor draining LNs suggest an important role of this subpopulation in pathological lymphangiogenesis.

Altogether, our study demonstrates an unprecedented implication of AXL in pathological lymphangiogenesis and particularly in tumor-draining LN where it is specifically produced by $MARCO^+$ LECs. Interestingly, AXL was found to influence LEC properties by amplifying VEGF-C mediated AKT pathway. AXL may thus represent a potential target to be considered in further studies for controlling pathological lymphangiogenesis.

Materials and methods

Cell culture, treatment, and transfection

Primary human LECs were obtained from Lonza (HMVEC-dLy, Bâle, Switzerland). Cells were grown in EBM-2 Endothelial Cell Growth Medium containing SingleQuots supplements (EGM^{TM}-2 kit, Lonza). Cells were treated without (control condition) or with bioactive form of rhVEGF-C (103-227aa) (Abcam, Cambridge, UK), rhVEGF-A (R&D Systems, Minneapolis, Minnesota, USA), rhVEGF-$C_{cys156ser}$ (R&D Systems), rhGAS6 (R&D Systems), rhHGF (R&D Systems) at 400ng/mL during the indicated time in serum-free EBM-2 medium. In some assays, cells were incubated with Mitomycin C (10 µg/mL, Sigma Life Science, Saint-Louis, MO, USA). The B16-F10 Luc tumor cell line was obtained from Caliper Life Sciences (Hopkinton, Massachusetts, USA). Cancer cells were grown in Dulbecco's modified Eagle's medium (DMEM, 10938-025, Thermo Fisher Scientific, Waltham, Massachusetts, USA) supplemented with 10% fetal bovine serum (Thermo Fisher Scientific), 1% glutamine (Thermo Fisher Scientific) and 1% penicillin–streptomycin (Thermo Fisher Scientific). All cells were incubated in a gas incubator set at 20% oxygen, 5% carbon dioxide and 37 °C.

AXL inhibition in in vitro experiments was performed using R428 (Gentaur ApexBio, London, UK) at different concentrations depending on the experimental settings (see details on figures or captions). DMSO treatment was used as a control condition.

ON-TARGETPlus siRNAs (for AXL and negative control) were purchased from Dharmacon (A). Three distinct non-targeting siRNAs were used as control (siCTRL 1: 5'-CAGAACUAGAUUGCGAAUA-3'; siCTRL 2: 5'-GCCCAAAUAAUGGUCAGAA-3'; siCTRL 3: 5'-GAUACUAUCUAGUCUAGAC-3') and three others were used to target AXL (siAXL 1: 5'- GACAUCCUCUUUCUCCUGC −3'; siAXL 2: 5'- GAUUUGGAGAACACACUGA −3'; siAXL 3: 5'- CAAGAUUCUAGAUGAUUAA −3'). Cells were plated and transfected at 50–70% confluency during 30 h, with a pool of the 3 siRNAs (20nM) using INTERFERin® reagent according to the manufacturer's protocole (Polyplus, Illkirch, France).

RT-qPCR

Total LEC RNA was isolated using the High Pure RNA isolation Kit (Roche, Bâle, Switzerland) according to the

manufacturer's instructions. RNAs (1 µg) were reverse-transcribed with the Transcriptor First Strand cDNA Synthesis Kit (Roche), and PCR was performed using SYBR Green Master mix II (Applied Biosystems, Waltham, USA). All reactions were done in triplicate using QuantStudio 3 Real-Time PCR system (Thermo Fisher Scientific), and expression levels calculated using comparative CT method (2^ΔΔCT). Gene expression levels were normalized to GAPDH level. The following primers from Eurogentec (Liege, Belgium) were used: 5'-ACCAGGTGGTCTCCTC TGAC-3' (GAPDH forward primer), 5'- TGCTGTAGCCA AATTCGTTG-3' (GAPDH reverse primer), 5'-GTGGCTG TGAAGACGATGAA-3' (AXL forward primer), 5'-ATGC AGACCGCTTCACTCA-3' (AXL reverse primer).

Western blotting

Cells were lysed with cell lysis buffer (Cell Signaling Technology, Danvers, Massachusetts, USA) containing phosphatase and protease inhibitors (Complete and phosSTOP; Roche, Bâle, Switzerland). Proteins were separated on acrylamide gels (8% or 10%) and transferred onto PVDF membranes. Proteins were detected by overnight incubation at 4 °C with the indicated primary antibodies followed by 1 h incubation at room temperature with horseradish peroxidase-coupled secondary antibody and enhanced chemiluminescent substrate (PerkinElmer, Waltham, USA) using a ImageQuant 800 imager (GE HealthCare, Chicago, Illinois, USA). The following antibodies were used: anti-AXL (Cell Signaling Technology Cat# 8661, RRID: AB_11217435), anti-pAXL (Tyr702, Cell Signaling Technology Cat# 5724, RRID: AB_10544794), anti-pAKT (Ser473, Cell Signaling Technology Cat# 9271 (also 9271 S, 9271 L, NYUIHC-310), RRID: AB_329825), anti-AKT (Cell Signaling Technology Cat# 9272 (also 9272 S), RRID: AB_329827), anti-VEGFR-2 (Cell Signaling Technology Cat# 2479 (also 2479 L, 2479 S), RRID: AB_2212507) (for all aforementioned antibodies, 1/1000), anti-VEGFR-3, anti-GAPDH (1/10,000; Millipore Cat# MAB374, RRID: AB_2107445), anti-rabbit (Cell Signaling Technology Cat# 7074 (also 7074 S, 7074 V, 7074P2), RRID: AB_2099233) and anti-mouse IgGs (Cell Signaling Technology Cat# 7076 (also 7076 S, 7076 V, 7076P2), RRID: AB_330924). When analyzing phosphorylated and total forms of a protein, blots were stripped and reprobed. Blots were run on parallel gels when proteins of similar molecular weight were analyzed. The western blot quantification was performed with the ImageJ software (RRID: SCR_003070) and Fiji (RRID: SCR_002285) software. All experiments analyzed by western blotting (Figs. 1 and 3B-D, Fig. S5) were performed at least 3 times. The complete kinetic analysis of pAXL (Fig. 3A) was performed only once but pAXL analysis at T0 and T30 was performed 3 times, confirming the results of the kinetic.

2D-migration assay by scratch wound healing

LECs (3×10^5) were seeded in 12-well plates. At confluence and after starvation, each well was wounded by creating a scratch with a plastic 200 µL tip on the cell monolayer. Images of scratch wounds were captured using phase-contrast inverted microscope (Nikon Eclipse Ti1, Tokyo, Japan; 10X magnification) at 0 h and 24 h after wounding. Wound area measurements at time 24 h were subtracted from wound area at time 0 h to quantify the area wound closure with the help of ImageJ software (RRID: SCR_003070) and Fiji (RRID: SCR_002285).

3D-migration assay (Spheroid sprouting assay)

Briefly, LECs were treated (30 min at 37 °C) with 0.5 µM fluorescent Green CMFDA dye (Life Technologies, Carlsbad, Californie, États-Unis) to counterstain the cytoplasm and with 0.5 µM SPY-650 DNA dye (Tebubio, Le-Perray-en-Yvelines, France) to counterstain the nuclei. Cells were washed, harvested and counted with CytoSmart Lux 3 system (Corning, Corning, New York, USA). For spheroid formation, LECs (3×10^3) were seeded in 96 well Cellstar U-bottom plates in suspension culture (Greiner Bio-One, Vilvoorde, Belgium) in EBM-2 complete medium supplemented with methylcellulose (0.75 mg/mL, Sigma-Aldrich, Saint-Louis, USA). A day after spheroid formation, spheroids were individually embedded in interstitial type I collagen gel (2 µg/µL, Corning) on 35 mm glass bottom dishes (ibidi GmbH, Gräfelfing, Germany). Collagen gel was polymerized at 20 °C for 30 min and at 37 °C for 30 additional min. EBM-2 complete medium and the different treatments were added on spheroid for 48 h. Z-stack images of spheroids were captured using a fluorescent confocal microscope (LSM880; Zeiss, Oberkochen, Germany; 10X magnification). Image processing sprout measurements (number and length) and quantifications for each spheroid were performed by a computer-assisted method using the image analysis toolbox of Matlab R2021a (Matworks, Inc., Natick, MA, USA, RRID: SCR_001622) as previously described [39].

Caspase assays

The activation of executioner caspase-3 in LECs was determined with the Caspase-Glo 3/7 Assay kit (Promega, Madison, Wisconsin, USA) according to the manufacturer's instructions. Cells were seeded in 96 well plate and the caspase substrate was directly added in well. Luminescence

was quantified after 30 min at 37 °C on SpectraMax i3 (Molecular Devices, San José, California, USA).

Immunoprecipitation

LEC lysates were obtained using lysis buffer (Cell Signaling Technology) containing phosphatase and protease inhibitors (Cell signaling), and AXL was immunoprecipitated by incubation for 30 min under rotation with Dynabeads Protein G (Thermo Fisher Scientific), on which AXL antibody (R&D Systems Cat# AF154, RRID: AB_354852, 1/1000) was previously bound. A flow through fraction of non-bound protein sample was collected for each timepoints, and beads were washed three times with PBS-Tween 0.02%. AXL and its partners were eluted in cell lysis buffer and heated at 95 °C for 5 min. Protein samples were then subjected to Western blotting. As a control, a corresponding goat IgG Isotype antibody (R&D Systems Cat# AB-108-C, RRID: AB_354267) was used instead of the specific antibody during immunoprecipitation.

Mice

C57Bl/6 mice (6- to 8-week-old) from Janvier Labs (Le Genest-Saint-Isle, France) were used throughout this study. The animals were maintained under a 12-h light-dark cycle with free access to food and water.

In vivo lymphangiogenesis assay: cell-free ear sponge assays

Gelatin sponges (Gelfoam, Pfizer, New York, USA) were cut into small pieces (3 mm^3) and incubated with PBS alone or with VEGF-C (1 µg, rhVEGF-C, Abcam). The sponges were then embedded in interstitial Type I collagen gel (1.5 mg/ml, Corning) and next implanted between the external ear skin layer and the cartilage of mouse ears as described previously [27]. All treatments (PBS with DMSO alone, DMSO or different doses of R428 (Gentaur Apex-Bio) from 1.9 ng, 3.8 ng or 7.6 ng with VEGF-C) were also injected every three days within the ear-implanted sponges until the end of the experiment at day 15. At the end of the assay, LNs were collected, incubated in 4% formol (VWR International, Radnor, Pennsylvania, USA) for 4 h, dehydrated in ethanol and embedded in paraffin (Leica Biosystems, Wetzlar, Germany).

In vivo tumor-associated lymphoangiogenesis assay: tumor-cell containing ear sponge assays

Gelatin sponges (Gelfoam, Pfizer, New York, USA) were cut into small pieces (3 mm^3) and incubated with either tumor cells (2×10^5 B16F10 cells/sponge) suspended in serum free-DMEM or serum-free DMEM (as control) alone for 30 min, embedded in Type I collagen gel (1.5 mg/ml; Corning) and implanted into mouse ears as previously described [27, 40]. After 28 days (=metastatic condition), LNs were collected and either embedded in tissue Tissue-Tek OCT (VWR International) and frozen at −80 °C or incubated in 4% formol (VWR International) for 4 h, dehydrated in ethanol and fixed in paraffin (Leica Biosystems).

Immunostainings of mice samples

Lymph node cryosections (5 µm) were fixed in 4% formol (VWR International) for 10 min. The paraffin Sect. (10 µm) were deparaffinized/rehydrated, and antigen retrieval was achieved by microwaved treatment in citrate buffer (Dako, Glostrup, Denmark) for 11 min at 126 °C. Then, both type sections were permeabilized for 5 min with 1% Triton X-100 (Millipore) at room temperature and blocked for 20 min in Animal-Free blocking solution (Cell signaling). Paraffin sections were incubated with LYVE-1 (R&D Systems Cat# AF2125, RRID: AB_2297188) antibody for 1 h at room temperature. After washing with PBS, anti-goat Alexa Fluor 488 antibody (Thermo Fisher Scientific Cat# A-11055 (also A11055), RRID: AB_2534102, 1/200) was added for 30 min at room temperature.

Cryosections were incubated at room temperature for 1 h with AXL and MARCO (Bio-Rad Cat# MCA1849T, RRID: AB_2140591, 1/200) antibodies. After washing with PBS, anti-goat Alexa Fluor 750 (Abcam Cat# ab175745, RRID: AB_2924800, 1/400) and anti-rat Alexa Fluor 647 (Thermo Fisher Scientific Cat# A-21472, RRID: AB_2535875, 1/500) secondary antibodies were added for 30 min at room temperature. In second step, LYVE-1 (Thermo Fisher Scientific Cat# 53-0443-82, RRID: AB_1633415) antibody conjugated to Alexa Fluor 488 was added after washing with PBS for 1 h. Finally, all sections were rinsed with PBS and then mounted with DAPI fluoromount-G (Southern Biotechnology Associates, Birmingham, Alabama, USA). At least 8 images per LN were used for staining density and distribution analysis. Images were acquired with the SLIDEVIEW VS200 research slide scanner (Olympus, Antwerpen, Belgium) equipped with a UPlan-XApo 20X objective (Olympus). The computerized quantifications were performed using the image analysis toolbox of Matlab R2021a (Matworks, Inc., Natick, MA, USA, RRID: SCR_001622) as previously described [41].

RNAscope assay

Prox1 mRNA were labelled according to the manufacturer's instructions (Advanced Cell Diagnostics, Bioké, Leiden, The Netherlands) on LN sections, as previously described [42]. Probes against *Prox1* mRNA were obtained from the manufacturer. After hybridization, the sections were incubated with AXL antibody (R&D Systems Cat# AF854, RRID: AB_355663, 1/75). After washing with PBS, anti-goat antibody conjugated with HRP (Millipore Cat# AP180P, RRID: AB_92573, 1/1000) was added for 30 min at room temperature. Staining was amplified using tyramide signal amplification working solution (TSA, PerkinElmer, Waltham, Massachusetts, USA) containing Cyanin 3 for 10 min. Finally, the sections were rinsed with PBS and then mounted with DAPI fluoromount-G (Southern Biotechnology Associates, Birmingham, Alabama, USA). Images were acquired with a fluorescent confocal microscope (LSM880; Zeiss, Oberkochen, Germany; 40X magnification).

Statistical analysis

Statistical analysis was performed with GraphPad Prism 9 (RRID: SCR_002798) or Matlab R2021a. QQ plots were performed to ensure the normal distribution of all data sets. Taking the group and parameter numbers into account, we conducted various parametric (1) or non-parametric (2) statistical tests, as specified in the legends. These included (1) the two-way or one-way ANOVA test, followed by multiple comparisons using Holm-Šídák correction, the unpaired t test or the one sample t-test. Subsequently, the data were presented as means ± SEM, with SEM representing the standard error of the mean and (2) the Kruskal-Wallis test followed by Dunn's multiple comparisons test, or the Mann-Whitney U test. The data were then represented as medians and interquartile ranges. Statistical significance was determined at a p-value less than 0.05, denoted as follows: *$p<0.05$, **$p<0.01$, ***$p<0.001$, ****$p<0.0001$."

Supplementary Information The online version contains supplementary material available at https://doi.org/10.1007/s00018-024-05542-3.

Acknowledgements The authors are grateful for the help of the GIGA-Imaging, and the GIGA-Mouse facility and Transgenics platform. We acknowledge the technical support of Emilie Feyereisen, Isabelle Dasoul, Erika Konradowski, Laetitia Montero-Ruiz and Nathalie Lefin.

Author contributions S.P, M.G.-I., L.B., L.R., J.D., S.Be. and A.N. designed and conducted the experiments. A.V. and C.G. determined the choice and efficiency of siRNA against AXL and tested the different AXL antibodies. F.G. and A.L. contributed to the setup of immunoprecipitation and immunohistological analyses. F.B and E.I helped with spheroid assay and western blot analyses. S.P., M.G.-I., B.S., S.B, C.G. and A.N. analyzed and interpreted the data. S.P., M.G.-I., A.N. and CG wrote the manuscript. A.N. designed the study and provided financial support. All authors revised the manuscript.

Funding This work was supported by grants from the Walloon Region through the FRFS-WELBIO strategic research program (WELBIO-CR-2019 A–03R), the Fonds de la Recherche Scientifique - FNRS (F.R.S.-FNRS, Belgium) T.0026.14, the FWO and F.R.S.-FNRS under the Excellence of Science programme (EOS No. 0.0037.22), the Fondation contre le Cancer (Foundation of Public Interest, Belgium), the Fonds spéciaux de la Recherche (University of Liège), the Centre Anticancéreux près l'Université de Liège, the Fonds Léon Fredericq (University of Liège), the Fondation Hospitalo Universitaire Léon Fredericq (FHULF, University of Liège), the PROTHERWAL project No. 7289 from the "Direction Générale Opérationnelle de l'Economie", the Wallonia-Brussels Federation (grant for Concerted Research Actions), and "Direction General de l'Organisation des Soins" (DGOS) funding of CRMR. This project has received funding from the European Union's Horizon 2020 research aid innovation program under grant agreement No 874708 (Theralymph). L.R., F.G. and J.D. are supported by a F.R.S.-FNRS-Télévie grant, S.B. by FRIA-FNRS, L.B. by F.R.S.-FNRS and C.G. is a Senior Research Associate at the F.R.S.-FNRS.

Data availability The datasets generated during and/or analyzed during the current study are available from the corresponding author on reasonable request.

Declarations

Ethical approval Animal experiments were performed in compliance with the Animal Ethical rules of the University of Liège (Liège, Belgium) after approval of the local Animal Ethical Committee (N°21-2361 and 17-1993).

Consent to participate Not applicable.

Consent to publish Not applicable.

Competing interests The authors declare that no conflict of interest exists.

References

1. Gillot L, Baudin L, Rouaud L et al (2021) The pre-metastatic niche in lymph nodes: formation and characteristics. Cell Mol

Life Sci CMLS 78:5987–6002. https://doi.org/10.1007/s00018-021-03873-z
2. Alitalo K (2011) The lymphatic vasculature in disease. Nat Med 17:1371–1380. https://doi.org/10.1038/nm.2545
3. Stacker SA, Williams SP, Karnezis T et al (2014) Lymphangiogenesis and lymphatic vessel remodelling in cancer. Nat Rev Cancer 14:159–172. https://doi.org/10.1038/nrc3677
4. Karaman S, Detmar M (2014) Mechanisms of lymphatic metastasis. J Clin Invest 124:922–928. https://doi.org/10.1172/JCI71606
5. Maus RLG, Jakub JW, Hieken TJ et al (2019) Identification of novel, immune-mediating extracellular vesicles in human lymphatic effluent draining primary cutaneous melanoma. https://doi.org/10.1080/2162402X.2019.1667742. OncoImmunology 8:
6. Dieterich LC, Tacconi C, Ducoli L, Detmar M (2022) Lymphatic vessels in cancer. Physiol Rev 102:1837–1879. https://doi.org/10.1152/physrev.00039.2021
7. Hood JL, San RS, Wickline SA (2011) Exosomes released by melanoma cells prepare sentinel lymph nodes for tumor metastasis. Cancer Res 71:3792–3801. https://doi.org/10.1158/0008-5472.CAN-10-4455
8. Cascinelli N, Morabito A, Santinami M et al (1998) Immediate or delayed dissection of regional nodes in patients with melanoma of the trunk: a randomised trial. WHO Melanoma Programme Lancet Lond Engl 351:793–796. https://doi.org/10.1016/s0140-6736(97)08260-3
9. Morton DL, Thompson JF, Cochran AJ et al (2014) Final Trial Report of Sentinel-Node Biopsy versus Nodal Observation in Melanoma. N Engl J Med 370:599–609. https://doi.org/10.1056/NEJMoa1310460
10. Nathanson SD, Kwon D, Kapke A et al (2009) The role of lymph node metastasis in the systemic dissemination of breast cancer. Ann Surg Oncol 16:3396–3405. https://doi.org/10.1245/s10434-009-0659-2
11. Pereira ER, Kedrin D, Seano G et al (2018) Lymph node metastases can invade local blood vessels, exit the node, and colonize distant organs in mice. Science 359:1403–1407. https://doi.org/10.1126/science.aal3622
12. Brown M, Assen FP, Leithner A et al (2018) Lymph node blood vessels provide exit routes for metastatic tumor cell dissemination in mice. Science 359:1408–1411. https://doi.org/10.1126/science.aal3662
13. Takeda A, Salmi M, Jalkanen S (2022) Lymph node lymphatic endothelial cells as multifaceted gatekeepers in the immune system. Trends Immunol 0. https://doi.org/10.1016/j.it.2022.10.010
14. Abe Y, Sakata-Yanagimoto M, Fujisawa M et al (2022) A single-cell atlas of non-haematopoietic cells in human lymph nodes and lymphoma reveals a landscape of stromal remodelling. Nat Cell Biol 24:565–578. https://doi.org/10.1038/s41556-022-00866-3
15. Carpentier KS, Sheridan RM, Lucas CJ et al (2021) MARCO^{+} lymphatic endothelial cells sequester arthritogenic alphaviruses to limit viremia and viral dissemination. EMBO J 40:e108966. https://doi.org/10.15252/embj.2021108966
16. Sibler E, He Y, Ducoli L et al (2021) Single-Cell Transcriptional Heterogeneity of Lymphatic Endothelial Cells in Normal and Inflamed Murine Lymph Nodes. Cells 10:1371. https://doi.org/10.3390/cells10061371
17. Durré T, Morfoisse F, Erpicum C et al (2018) uPARAP/Endo180 receptor is a gatekeeper of VEGFR-2/VEGFR-3 heterodimerisation during pathological lymphangiogenesis. Nat Commun 9:5178. https://doi.org/10.1038/s41467-018-07514-1
18. Simons M, Gordon E, Claesson-Welsh L (2016) Mechanisms and regulation of endothelial VEGF receptor signalling. Nat Rev Mol Cell Biol 17:611–625. https://doi.org/10.1038/nrm.2016.87
19. Karaman S, Leppänen V-M, Alitalo K (2018) Vascular endothelial growth factor signaling in development and disease. Dev Camb Engl 145:dev151019. https://doi.org/10.1242/dev.151019
20. Morfoisse F, Noel A (2019) Lymphatic and blood systems: Identical or fraternal twins? Int J Biochem Cell Biol 114:105562. https://doi.org/10.1016/j.biocel.2019.105562
21. Martinez-Corral I, Zhang Y, Petkova M et al (2020) Blockade of VEGF-C signaling inhibits lymphatic malformations driven by oncogenic PIK3CA mutation. Nat Commun 11:2869. https://doi.org/10.1038/s41467-020-16496-y
22. Coso S, Zeng Y, Opeskin K, Williams ED (2012) Vascular endothelial growth factor receptor-3 directly interacts with phosphatidylinositol 3-kinase to regulate lymphangiogenesis. PLoS ONE 7:e39558. https://doi.org/10.1371/journal.pone.0039558
23. Ruan G-X, Kazlauskas A (2012) Axl is essential for VEGF-A-dependent activation of PI3K/Akt. EMBO J 31:1692–1703. https://doi.org/10.1038/emboj.2012.21
24. Tanaka M, Siemann DW (2020) Gas6/Axl Signaling Pathway in the Tumor Immune Microenvironment. Cancers 12:1850. https://doi.org/10.3390/cancers12071850
25. Varnum BC, Young C, Elliott G et al (1995) Axl receptor tyrosine kinase stimulated by the vitamin K-dependent protein encoded by growth-arrest-specific gene 6. Nature 373:623–626. https://doi.org/10.1038/373623a0
26. Paul MD, Hristova K (2019) The RTK Interactome: Overview and Perspective on RTK Hetero-Interactions. Chem Rev 119:5881–5921. https://doi.org/10.1021/acs.chemrev.8b00467
27. García-Caballero M, Van de Velde M, Blacher S et al (2017) Modeling pre-metastatic lymphvascular niche in the mouse ear sponge assay. Sci Rep 7:41494. https://doi.org/10.1038/srep41494
28. Nassar M, Tabib Y, Capucha T et al (2017) GAS6 is a key homeostatic immunological regulator of host-commensal interactions in the oral mucosa. Proc Natl Acad Sci U S A 114:E337–E346. https://doi.org/10.1073/pnas.1614926114
29. Petrova TV, Mäkinen T, Mäkelä TP et al (2002) Lymphatic endothelial reprogramming of vascular endothelial cells by the Prox-1 homeobox transcription factor. EMBO J 21:4593–4599. https://doi.org/10.1093/emboj/cdf470
30. Chai Z-T, Zhang X-P, Ao J-Y et al (2021) AXL Overexpression in Tumor-Derived Endothelial Cells Promotes Vessel Metastasis in Patients With Hepatocellular Carcinoma. Front Oncol 11:650963. https://doi.org/10.3389/fonc.2021.650963
31. Holland SJ, Powell MJ, Franci C et al (2005) Multiple roles for the receptor tyrosine kinase axl in tumor formation. Cancer Res 65:9294–9303. https://doi.org/10.1158/0008-5472.CAN-05-0993
32. Huang M, Liu M, Huang D et al (2022) Tumor perivascular cell-derived extracellular vesicles promote angiogenesis via the Gas6/Axl pathway. Cancer Lett 524:131–143. https://doi.org/10.1016/j.canlet.2021.10.023
33. Wu G, Ma Z, Cheng Y et al (2018) Targeting Gas6/TAM in cancer cells and tumor microenvironment. Mol Cancer 17:20. https://doi.org/10.1186/s12943-018-0769-1
34. Van de Velde M, García-Caballero M, Durré T et al (2018) Ear Sponge Assay: A Method to Investigate Angiogenesis and Lymphangiogenesis in Mice. Methods Mol Biol Clifton NJ 1731:223–233. https://doi.org/10.1007/978-1-4939-7595-2_20
35. Goyette M-A, Duhamel S, Aubert L et al (2018) The Receptor Tyrosine Kinase AXL Is Required at Multiple Steps of the Metastatic Cascade during HER2-Positive Breast Cancer Progression. Cell Rep 23:1476–1490. https://doi.org/10.1016/j.celrep.2018.04.019
36. del Pozo Martin Y, Park D, Ramachandran A et al (2015) Mesenchymal Cancer Cell-Stroma Crosstalk Promotes Niche Activation, Epithelial Reversion, and Metastatic Colonization. Cell Rep 13:2456–2469. https://doi.org/10.1016/j.celrep.2015.11.025
37. Holland SJ, Pan A, Franci C et al (2010) R428, a selective small molecule inhibitor of Axl kinase, blocks tumor spread and

prolongs survival in models of metastatic breast cancer. Cancer Res 70:1544–1554. https://doi.org/10.1158/0008-5472.CAN-09-2997
38. Kim M-S, Zhong Y, Yachida S et al (2014) Heterogeneity of pancreatic cancer metastases in a single patient revealed by quantitative proteomics. Mol Cell Proteom MCP 13:2803–2811. https://doi.org/10.1074/mcp.M114.038547
39. Blacher S, Erpicum C, Lenoir B et al (2014) Cell Invasion in the Spheroid Sprouting Assay: A Spatial Organisation Analysis Adaptable to Cell Behaviour. PLoS ONE 9:e97019. https://doi.org/10.1371/journal.pone.0097019
40. Nowak-Sliwinska P, Alitalo K, Allen E et al (2018) Consensus guidelines for the use and interpretation of angiogenesis assays. Angiogenesis 21:425–532. https://doi.org/10.1007/s10456-018-9613-x
41. Maertens L, Erpicum C, Detry B et al (2014) Bone marrow-derived mesenchymal stem cells drive lymphangiogenesis. PLoS ONE 9:e106976. https://doi.org/10.1371/journal.pone.0106976
42. Gillot L, Lebeau A, Baudin L et al (2022) Periostin in lymph node pre-metastatic niches governs lymphatic endothelial cell functions and metastatic colonization. Cell Mol Life Sci CMLS 79:295. https://doi.org/10.1007/s00018-022-04262-w